ChemComm

COMMUNICATION

View Article Online
View Journal | View Issue

Cite this: *Chem. Commun.*, 2018, **54**, 11029

Received 11th July 2018,
Accepted 5th September 2018

DOI: 10.1039/c8cc05615c

rsc.li/chemcomm

Graphene oxide-wrapped dipotassium terephthalate hollow microrods for enhanced potassium storage†

Xuanpeng Wang,‡ Kang Han,‡ Chenyang Wang,‡ Ziang Liu, Xiaoming Xu, Meng Huang, Ping Hu, Jiashen Meng, Qi Li* and Liqiang Mai *

Unique graphene oxide-wrapped organic dipotassium terephthalate hollow microrods were synthesised using an abundant and renewable organic resource. They exhibit enhanced potassium storage compared to bulk K_2TP, which can be ascribed to the fast K^+ ion transfer kinetics, high electronic conductivity and short diffusion distance.

In order to realize the sustainable development of modern society, searching for efficient energy storage systems with characteristics of high capacity, long cycling life, low cost and reliable security has become an urgent issue for human beings.[1,2] Lithium-ion batteries (LIBs) currently dominate the intelligent electronic device market and grid storage due to their unique energy storage properties.[3–5] However, the energy storage ability of commercial LIBs is greatly dependent on conventional Li-containing inorganic electrodes, and their specific capacities mean they can rarely achieve dramatic breakthroughs. Moreover, the increasing scarcity and uneven geographical distribution of lithium resources bring about cost rises, especially for large-scale electrical grid application. Therefore, more and more attention is paid to alternative candidates, such as sodium-ion batteries (NIBs) and potassium-ion batteries (KIBs) due to the abundance of Na and K elements in the Earth's crust (~2.09 wt% of K, 2.36 wt% of Na and 0.0017 wt% of Li).[6,7]

KIBs exhibit attractive advantages due not only to the high abundance of potassium, but also due to the similar redox potential of K^+/K (−2.94 V *vs.* SHE) to the Li^+/Li couple (−3.04 V *vs.* SHE), which is around 200 mV lower than that of the Na^+/Na couple (−2.71 V *vs.* SHE).[8–10] This means that the voltage and energy density in KIBs can be higher than those in NIBs in the case of the same electrode systems. Furthermore, K^+ has much weaker Lewis acidity than Li^+ and Na^+, which endows a smaller Stoke's radius of solvated ions in liquid electrolyte, ultimately resulting in a larger transport number and higher mobility of K^+ ions in electrolyte and at the electrode/electrolyte interface.[6,11] Nevertheless, K is much more active than Li and Na, which could cause more serious accidents once K dendrites come into being while the batteries are running. Besides, the larger ionic radius of K^+ will lead to larger polarization and volume expansion. Thus, the key to the development of KIBs is seeking suitable electrode materials to accommodate the large K^+ ions, with high safety and a stable framework structure. For anodes, carbon-based materials have been studied due to their low cost and excellent electric conductivity.[12–14] Graphite shows an encouraging depotassiation capacity, but poor cycling stability caused by the large and inevitable volume expansion of graphite (about 61%) as a result of the large radius of K^+ ion.[12] In particular, it is worth noting that carbon anodes exhibit an average discharge plateau of 0.3 V *vs.* K^+/K, at which the risk of dendrite formation will increase, bringing about severe safety hazards.[11] Hence, there is an urgent demand to seek anodes with stable cyclability and high safety for KIBs.

Recently, organic compounds have gradually achieved immense priority over inorganic materials for their manageable structures, suitable operating voltage and abundance as well as renewability.[15–22] In particular, compared with inorganic solids, which are constructed with covalent/ionic bonds, the crystal state of organic materials is mainly governed by van der Waals forces, which can provide more active sites as well as a lower energy barrier for accommodation of K^+ ions without size concerns.[6,23] However, their electrochemical performance is subject to intrinsic poor conductivity and solubility in organic electrolyte.[10] On one hand, nanotechnology and conductive coatings are considered the most effective methods to enhance their conductivity. On the other hand, the solubility can be significantly retarded by turning the organic materials into their corresponding organic salts, coating with a non-active passivation layer and exploring suitable electrolytes.[6,11,24–27] Dipotassium terephthalate (K_2TP) is a typical organic material with two conjugated carboxylate groups, which become stable with a two K^+ insertion/extraction. Moreover, K_2TP possesses a suitable and constant operating potential of about ~0.6 V *vs.* K^+/K when tested as an anode for KIBs, which

State Key Laboratory of Advanced Technology for Materials Synthesis and Processing, Wuhan University of Technology, Wuhan 430070, China. E-mail: qi.li@whut.edu.cn, mlq518@whut.edu.cn

† Electronic supplementary information (ESI) available: Experimental details and supplementary figures. See DOI: 10.1039/c8cc05615c

‡ X. P. Wang, K. Han and C. Y. Wang contributed equally to this work.

can avoid the formation of K dendrites and the corresponding safety concerns.[6,23,27] Recently, Li's group revealed that K_2TP with a theoretical capacity of 221 mA h g^{-1} and two conjugated carboxylate groups can be regarded as a potential anode for KIBs, in which it delivers a considerable capacity of 181 mA h g^{-1} at a rate of 0.2C.[6] However, owing to its inherent poor electronic conductivity, the rate capacity and cell cyclability still need further improvement.

Herein, we synthesized graphene oxide-wrapped organic dipotassium terephthalate (K_2TP@GO) hollow microrods with highly stable cycling, good rate capability, and high safety. Firstly, the electronic conductivity is greatly enhanced by graphene oxide modification. Secondly, the graphene oxide surface coating can serve as a buffer layer to probably not just alleviate the active materials' volume expansion, but also restrain the dissolution during the discharge/charge processes.[10] Thirdly, the unique hollow structure promotes K^+ transportation and provides enough inner space to accommodate volume expansion during depotassiation/potassiation processes. Moreover, on the basis of *in situ* X-ray diffraction (XRD) analysis, the structural evolution and potassium storage mechanism were convincingly revealed, and it was confirmed that the K_2TP@GO demonstrated highly reversible properties during depotassiation/potassiation processes. This work may offer a solution for the construction of high performance organic anodes with abundant and renewable sources for new-type KIBs.

The synthetic process of K_2TP@GO is depicted in Fig. 1A. The XRD patterns of the as-obtained K_2TP@GO and bulk K_2TP were obtained, as shown in Fig. 1B, and are well consistent with the standard card (JCPDS No. 00-052-2142). Owing to the integrative action of the electrostatic attraction/chemical bond between the aromatic nucleus and metal cations as well as the stable benzene skeleton with large π conjugation,[10,28–30] K_2TP exhibits good thermal stability, possessing a high thermal decomposition temperature of over 550 °C which is much higher than that of terephthalic acid (PTA) (300 °C) (Fig. S1, ESI†). Fourier-transform infrared (FT-IR) spectra are shown in Fig. 1C and the broad peak between 2400 and 3000 cm^{-1} is assigned to the stretching vibration of O–H while the bands located at 1681 and 1284 cm^{-1} are assigned to ν_s(COO–) and ν_{as}(COO–) vibrations in PTA. The typical absorption peaks located at 1572 and 1377 cm^{-1} are ascribed to the formation of K_2TP.[24] The morphology features of the synthesized hollow K_2TP@GO microrods were observed using a scanning electron microscope (SEM) (Fig. 1D and E). Hollow K_2TP@GO microrods exhibit micro sizes in the range of 5–20 μm and single hollow K_2TP microrods are wrapped together by graphene oxide. The EDS element mapping results demonstrate the uniform distribution of K, C and O elements in K_2TP@GO (Fig. 1F). In addition, the morphology images of bulk-shaped K_2TP are displayed in Fig. S2 (ESI†).

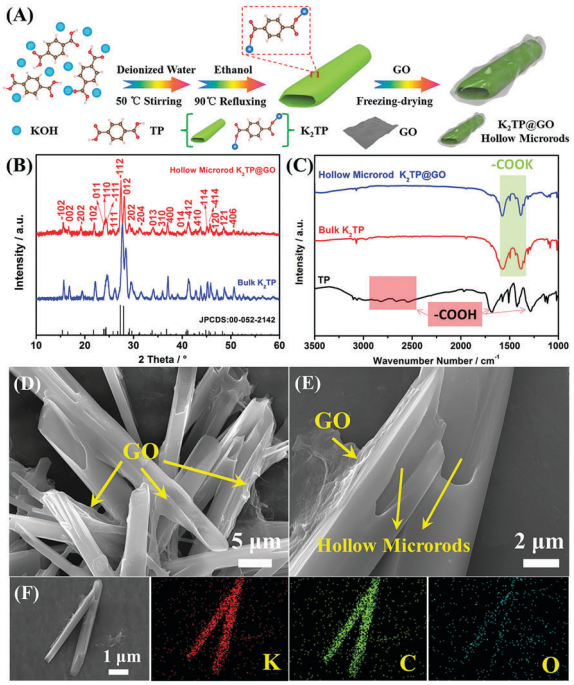

Fig. 1 (A) Schematic illustration of the preparation process for hollow K_2TP@GO microrods. Experimental XRD patterns (B), FT-IR spectra (C), SEM images (D and E) and EDS spectrum (F) of hollow K_2TP@GO microrods.

Fig. 2A displays the cyclic voltammetry (CV) measurements of the K_2TP@GO electrode, which displays redox peaks around 0.52/0.69 V (*vs.* K^+/K), corresponding to the insertion/extraction of two K-ions.[12,13] Except for the first scan, reversible and stable redox behaviour is observed, suggesting the reversibility of the K_2TP@GO anode. The lower reduction peak in the initial cycle can be ascribed to the formation of SEI.[11] For comparison, the CV curves of bulk K_2TP are depicted in Fig. S4 (ESI†). The selected discharge/charge galvanostatic cycling profiles of K_2TP@GO at a current density of 200 mA g^{-1} are presented in Fig. 2B. The charge and discharge voltages are located at around 0.68 and 0.52 V, with a small polarization of about 0.16 V. The polarization scarcely increases until the 100th cycle. The slope below 0.3 V present in the initial discharge process, which is in accordance with the CV curves, results from the formation of SEI during the K^+ insertion process.[6,11] Apparently, the bulk K_2TP electrode has much larger polarization, as shown in Fig. S5 (ESI†).

Fig. 2B and C illustrate the cycling performance and corresponding coulombic efficiency of K_2TP@GO and bulk K_2TP. As for K_2TP@GO, a reversible capacity of around 212 mA h g^{-1} is delivered at 200 mA g^{-1}, with a high capacity retention of 92.3% after 100 cycles. Remarkably, it achieves a coulombic efficiency as high as 99% except for in the first several cycles. The irreversible capacity and low coulombic efficiency of the first cycle results from the formation of SEI during the discharge process.[6,11,24,31] For bulk K_2TP, although it delivers capacities of 483.2 mA h g^{-1} and 176.6 mA h g^{-1} in the first two cycles at the same current density, it drops dramatically and a capacity of only 28 mA h g^{-1} is obtained after 100 cycles.

The rate capability of K_2TP@GO was also investigated at current densities varying from 50 to 1000 mA g^{-1}. As shown in Fig. 2E, it is worth noting that the K_2TP@GO electrode exhibits discharge capacities of 296, 252, 200, 150 and 114 mA h g^{-1} at current densities of 50, 100, 200, 500, and 1000 mA g^{-1}, respectively. When the current density is set back to 50 mA g^{-1}, the K_2TP@GO

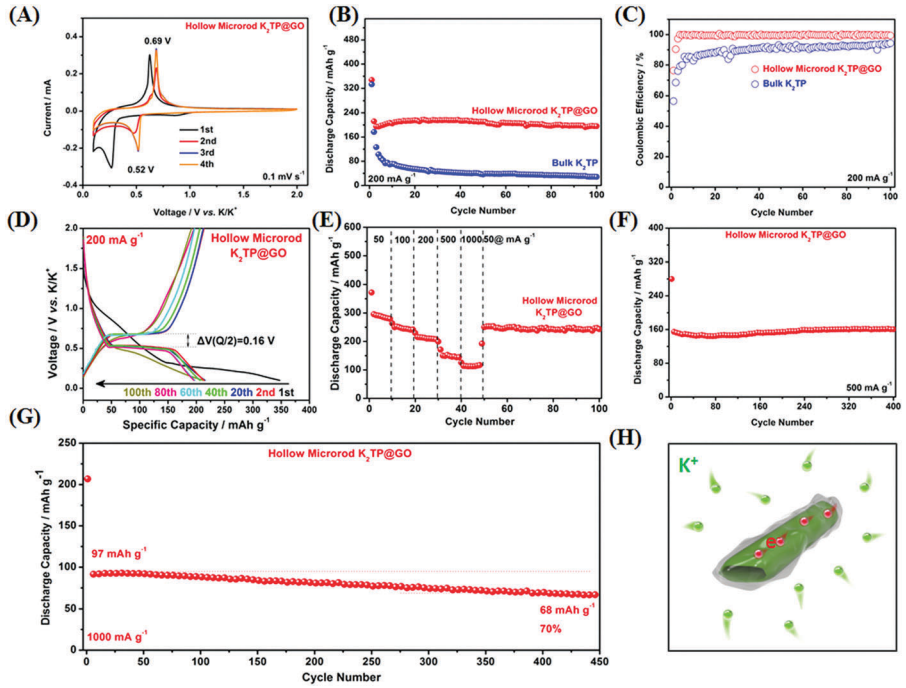

Fig. 2 Electrochemical performances of K_2TP@GO and K_2TP. (A) CV curves of K_2TP@GO in the initial four cycles were tested at a scan rate of 0.1 mV s^{-1} ranging from 0.1 to 2.0 V. Cycle performance (B) and the corresponding coulombic efficiency (C) of K_2TP@GO and bulk K_2TP electrodes at a current density of 200 mA g^{-1}. (D) Charge and discharge curves of K_2TP@GO at a current density of 200 mA g^{-1}. (E) Rate performance of K_2TP@GO at different rates. Long cycling measurements of K_2TP@GO tested at (F) 500 mA g^{-1} and 1000 mA g^{-1}. (H) Schematic illustration of K_2TP@GO with fast K^+ and electronic transportation and unique hollow structure with a graphene oxide wrapped layer.

electrode still achieves a stable reversible capacity of 256 mA h g^{-1}, suggesting good rate recovery and cycling stability. Nevertheless, the rate performance of bulk K_2TP, displayed in Fig. S6 (ESI†), is quite poor as its capacity decreases to almost zero when the current is increased to 1000 mA g^{-1}. Moreover, the corresponding discharge/charge curves at different current rates for K_2TP@GO and bulk K_2TP are shown in Fig. S7 (ESI†). Furthermore, the K_2TP@GO anode was cycled at high current densities of 500 and 1000 mA g^{-1} to evaluate its long-term cycling performance (Fig. 2F and G). When the current density is increased to 500 mA g^{-1}, the K_2TP@GO anode maintains a stable capacity of 160 mA h g^{-1} after 400 cycles, while the performance of the bulk K_2TP anode is extremely poor (Fig. S8, ESI†). It achieves a reversible capacity of 97 mA h g^{-1} at a current density of 1000 mA g^{-1} after several initial cycles, and the capacity retains a value of 68 mA h g^{-1} after 450 cycles (capacity retention rate of 70%). The coulombic efficiency of K_2TP@GO at 500 and 1000 mA g^{-1} is extremely high, achieving as much as 99% and demonstrating its good electrochemical reversibility (Fig. S9A and B, ESI†). A schematic illustration of K_2TP@GO with fast K^+ and electronic transportation and a unique hollow structure with graphene oxide wrapping is shown in Fig. 2H.

The superior rate capability of K_2TP@GO is attributed to the high transport rate of K^+ and improved electronic conductivity (Fig. S10–12, ESI†). In summary, the graphene oxide-wrapped layer and hollow structure can effectively enhance the electronic conductivity, accelerate K^+ transfer kinetics, improve structure stability and decrease the volume expansion, leading to the superior K^+ storage properties of K_2TP@GO (Table S1, ESI†).

In order to elucidate the potassium storage mechanism of K_2TP@GO, we performed electrochemical *in situ* XRD measurements (Fig. 3A and Fig. S13, ESI†). Two diffraction peaks located at ~21.9° and ~27.3° can be clearly observed, corresponding to the (102) and (−112) planes of K_2TP, respectively. Obviously, the two diffraction peaks indicate the same evolution of crystal structure during cycling. Upon the initial discharge process, the peaks weakened and gradually disappeared, indicating the transformation from a crystalline to an amorphous state ($K_2TP \rightarrow K_4TP$).[24] Nevertheless, when charged to 2.0 V, the peaks

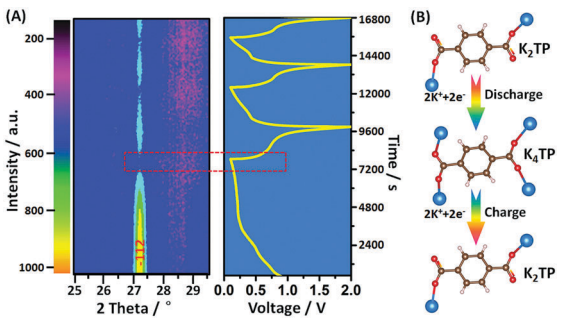

Fig. 3 (A) *In situ* XRD patterns of the K_2TP@GO electrode during the galvanostatic depotassiation/potassiation process at 100 mA g^{-1} and the image plot of the diffraction patterns at 25–29.5° during the first three cycles. (B) Schematic illustration of K^+ insertion/extraction in the K_2TP@GO electrode.

reappeared during the depotassiation process ($K_4TP \rightarrow K_2TP$). Similar behaviour is also observed in the following cycles. For the other three peaks, the changes (enhancement and broadening) during the first two cycles may be attributed to the volume expansion/contraction of the electrode, and no significant changes occur in subsequent cycles. The intensity becomes weaker in contrast to the first cycle, which is consistent with large capacity fading in the initial cycle stage. The structural evolution confirms that K_2TP@GO can demonstrate highly reversible properties during electrochemical potassiation/depotassiation processes. Moreover, this is a two electron transfer reaction as illustrated in Fig. 3B and Fig. S14 (ESI†), displaying a reversible conversion between the K_2TP phase and the K_4TP phase during K^+ insertion/extraction processes.

In conclusion, we synthesized graphene oxide-wrapped hollow potassium terephthalate microrods as highly efficient anodes in KIBs. K_2TP@GO hollow microrods display a high reversible capacity of 212 mA h g^{-1} at 200 mA g^{-1}, compared with bulk K_2TP. More impressively, a stable capacity of 160 mA h g^{-1} can be maintained at a high current density of 500 mA g^{-1} after 400 cycles. The superior K^+ storage properties are ascribed to fast K^+ transfer kinetics, high electronic conductivity and a robust hollow structure. In addition, the potassium storage mechanism of K_2TP@GO hollow microrods was revealed. During the potassiation process, the crystalline phase of K_2TP gradually transformed into amorphous K_4TP. This work investigates the rational design of K_2TP hollow microrods with enhanced K^+ storage performance and may stimulate further study of organic materials in KIBs.

This work was supported by the National Natural Science Fund for Distinguished Young Scholars (51425204), the National Natural Science Foundation of China (51832004, 21805219), the State Key Laboratory of Advanced Technology for Materials Synthesis and Processing (WUT: 2018-KF-1), the Fundamental Research Funds for the Central Universities (WUT: 2017IVA100, 2017IVA096), and the National Students Innovation and Entrepreneurship Training Program (WUT: 20171049701013). We thank Prof. Ali Javey of the University of California, Berkeley for strong support and stimulating discussions.

Conflicts of interest

There are no conflicts to declare.

Notes and references

1 L. Xue, Y. Li, H. Gao, W. Zhou, X. Lu, W. Kaveevivitchai, A. Manthiram and J. B. Goodenough, *J. Am. Chem. Soc.*, 2017, **139**, 2164–2167.
2 X. Wang, P. Hu, C. Niu, J. Meng, X. Xu, X. Wei, C. Tang, W. Luo, L. Zhou, Q. An and L. Mai, *Nano Energy*, 2017, **35**, 71–78.
3 J. Han, M. Xu, Y. Niu, G. N. Li, M. Wang, Y. Zhang, M. Jia and C. M. Li, *Chem. Commun.*, 2016, **52**, 11274–11276.
4 J. C. Pramudita, D. Sehrawat, D. Goonetilleke and N. Sharma, *Adv. Energy Mater.*, 2017, **7**, 1602911.
5 D. Lin, Y. Liu, W. Chen, G. Zhou, K. Liu, B. Dunn and Y. Cui, *Nano Lett.*, 2017, **17**, 3731–3737.
6 Q. Deng, J. Pei, C. Fan, J. Ma, B. Cao, C. Li, Y. Jin, L. Wang and J. Li, *Nano Energy*, 2017, **33**, 350–355.
7 S. Irin, R. Thrinathreddy, M. R. Md, C. Ying and M. G. Alexey, *Chem. Commun.*, 2016, **52**, 9279–9282.
8 X. Wang, X. Xu, C. Niu, J. Meng, M. Huang, X. Liu, Z. Liu and L. Mai, *Nano Lett.*, 2017, **17**, 544–550.
9 Y. Chen, W. Luo, M. Carter, L. Zhou, J. Dai, K. Fu, S. Lacey, T. Li, J. Wan, X. Han, Y. Bao and L. Hu, *Nano Energy*, 2015, **18**, 205–211.
10 C. Li, Q. Deng, H. Tan, C. Wang, C. Fan, J. Pei, B. Cao, Z. Wang and J. Li, *ACS Appl. Mater. Interfaces*, 2017, **9**, 27414–27420.
11 K. Lei, F. Li, C. Mu, J. Wang, Q. Zhao, C. Chen and J. Chen, *Energy Environ. Sci.*, 2017, **10**, 552–557.
12 Z. Jian, W. Luo and X. Ji, *J. Mater. Chem. A*, 2015, **137**, 11566–11569.
13 Z. Jian, Z. Xing, C. Bommier, Z. Li and X. Ji, *Adv. Energy Mater.*, 2016, **6**, 1501874.
14 A. Eftekhari, Z. Jian and X. Ji, *ACS Appl. Mater. Interfaces*, 2016, **9**, 4404–4419.
15 S. Wang, L. Wang, K. Zhang, Z. Zhu, Z. Tao and J. Chen, *Nano Lett.*, 2013, **13**, 4404–4409.
16 K. Sakaushi, E. Hosono, G. Nickerl, T. Gemming, H. Zhou, S. Kaskel and J. Eckert, *Nat. Commun.*, 2013, **4**, 1485.
17 S. Wang, L. Wang, Z. Zhu, Z. Hu, Q. Zhao and J. Chen, *Angew. Chem., Int. Ed.*, 2014, **53**, 5892–5896.
18 T. B. Schon, B. T. McAllister, P.-F. Li and D. S. Seferos, *Chem. Soc. Rev.*, 2016, **45**, 6345–6404.
19 Q. Zhao, J. Wang, Y. Lu, Y. Li, G. Liang and J. Chen, *Angew. Chem., Int. Ed.*, 2016, **55**, 1–6.
20 H. Wang, S. Yuan, D. Ma, X. Huang, F. Meng and X. Zhang, *Adv. Energy Mater.*, 2014, **4**, 1301651.
21 W. Luo, M. Allen, V. Raju and X. Ji, *Adv. Energy Mater.*, 2014, **4**, 1400554.
22 H. Kim, D.-H. Seo, G. Yoon, W. A. Goddard, Y. S. Lee, W.-S. Yoon and K. Kang, *J. Phys. Chem. Lett.*, 2014, **5**, 3086–3092.
23 Y. Y. Zhang, Y. Y. Sun, S. X. Du, H. J. Gao and S. B. Zhang, *Appl. Phys. Lett.*, 2012, **100**, 1176.
24 Q. Deng, C. Fan, L. Wang, B. Cao, Y. Jin, C.-M. Che and J. Li, *Electrochim. Acta*, 2016, **222**, 1086–1093.
25 F. Wan, X. Wu, J. Guo, J. Li, J. Zhang, L. Niu and R. Wang, *Nano Energy*, 2015, **13**, 450–457.
26 L. Zhao, J. Zhao, Y. Hu, H. Li, Z. Zhou, M. Armand and L. Chen, *Adv. Energy Mater.*, 2012, **2**, 962–965.
27 K. Lei, F. Li, C. Mu, J. Wang, Q. Zhao, C. Chen and J. Chen, *Energy Environ. Sci.*, 2017, 10.
28 T. Yasuda and N. Ogihara, *Chem. Commun.*, 2014, **50**, 11565–11567.
29 N. Ogihara, T. Yasuda, Y. Kishida, T. Ohsuna, K. Miyamoto and N. Ohba, *Angew. Chem., Int. Ed.*, 2014, **53**, 11467–11472.
30 C. Wang, Y. Xu, Y. Fang, M. Zhou, L. Liang, S. Singh, H. Zhao, A. Schober and Y. Lei, *J. Am. Chem. Soc.*, 2015, **137**, 3124–3130.
31 Y. Wang, K. Kretschmer, J. Zhang, A. K. Mondal, X. Guo and G. Wang, *RSC Adv.*, 2016, **6**, 57098–57102.

